NJC

New Journal of Chemistry

A journal for new directions in chemistry

Accepted Manuscript

This article can be cited before page numbers have been issued, to do this please use: S. A. A. Noma, A. Ulu, O. Acet, R. Sanz, E. S. Sanz, M. Odabasi and B. Ates, *New J. Chem.*, 2020, DOI: 10.1039/D0NJ00127A.

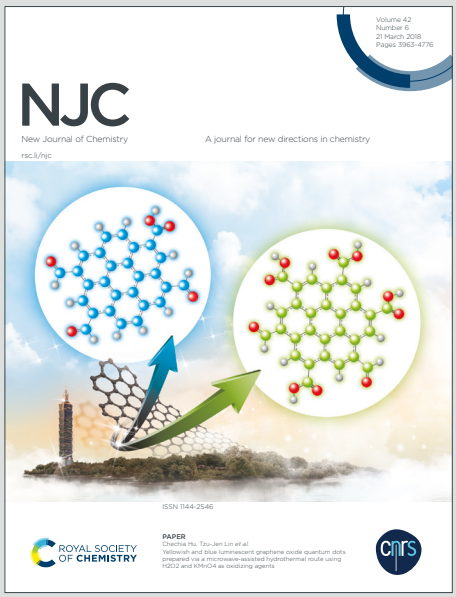

Comparative study of ASNase Immobilization on Tannic Acid-Modified Magnetic Fe_3O_4/SBA-15 Nanoparticles to Enhance Stability and Reusability

Samir Abbas Ali Noma[1], Ahmet Ulu[1], Ömür Acet[2], Raúl Sanz[3], Eloy S. Sanz-Pérez[4], Mehmet Odabaşı[2], Burhan Ateş[1*]

[1]*Department of Chemistry, Science and Literature Faculty, İnönü University, 44280, Malatya, Turkey*

[2]*Aksaray University, Faculty of Arts and Science, Chemistry Department, Aksaray, Turkey*

[3]*Department of Chemical and Environmental Technology, ESCET, Universidad Rey Juan Carlos, C/ Tulipán s/n, 28933 Móstoles, Madrid, Spain*

[3]*Department of Chemical, Energy, and Mechanical Technology, ESCET, Universidad Rey Juan Carlos, C/ Tulipán s/n, 28933 Móstoles, Madrid, Spain*

*Corresponding Author: Burhan ATEŞ

E-mail: burhan.ates@inonu.edu.tr

Tel: (+) 90-422-3773888

Fax: (+) 90-422-3410037

Address: Department of Chemistry, Faculty of Arts and Science,

İnönü University, 44280, Malatya, Turkey

Abstract: In this work, L-asparaginase was immobilized on tannic acid-modified magnetic mesoporous particles. In brief, Fe_3O_4/SBA-15/tannic acid magnetic particles were synthesized and fully characterized by using various methods as structural and morphological. The properties of free and immobilized enzyme were examined in terms of pH, temperature, thermal stability, storage stability, and reusability. Moreover, the effects of metal ions, inhibitors and organic solvents were investigated on activity of the immobilized enzyme. As compared to free enzyme, the immobilized enzyme possessed better tolerance to changes in ambient temperature and pH. Additionally, thermal incubation results showed that free enzyme lost its activity while the immobilized enzyme exhibited the opposite behavior. Most strikingly, the immobilized L-asparaginase exhibited a high degree of activity (70%) after being reused 16 times while also demonstrating 71% and 63% storage stability of the initial activity even after 28 days, at 4 °C and room temperature, respectively. Together with these results, L-asparaginase was successfully immobilized upon Fe_3O_4/SBA-15/tannic acid magnetic nanoparticles with improved stability properties. This support holds great potential and opens up a novel perspective for its growing applications.

Keywords: Enzyme immobilization; Magnetic nanoparticles; Surface functionalization; Asparaginase; Tannic acid

1. Introduction

Enzyme immobilization is defined as the chemical and/or physical interaction of different types of carriers to reduce the mobility of free or dissolved enzyme. The immobilized enzyme is more stable than free enzyme against factors such as pH, high temperature, various denaturing organic solvents.[1] In recent years, immobilize enzyme technology has been commonly used in multidisciplinary studies for the analysis of medicine, antibiotic production, drug metabolism, food industry, biodiesel production, biosensor, bioremediation and clinical.[2,3] The most important problem encountered in soluble enzymes applications is rapid activity loss and high cost of some enzymes. Most importantly, the control of enzymes is very difficult and is impossible to remove the enzymes from the reaction medium. Therefore, various immobilization techniques such as adsorption, covalent binding, entrapment and crosslinking have been developed in order to improve enzyme activity.[2,4]

On the other hand, the choice of suitable carrier support material for enzyme immobilization has a critical role to ensure the performance and stabilization of the enzyme. In recent years, the trend supports commonly used for enzyme immobilization are nanoparticles and their modified forms. In this respect, SBA-15 (Santa Barbara Amorphous) produced in 1998 by Zhao et al. [5] has attracted high interest because of some properties such as high surface area, large pore volume, complement channels [6] and the combination of micro and mesoporous constructions.[7,8] These excellent structural and textural features, which make them very desired matrices for some implementations such as adsorption, catalysis and drug delivery.[9–11] And also, when compared to other particles, silica-based structures are non-toxic, biodegradable and relatively cheap. The main reasons for choosing SBA-15 in adsorption process are primarily to combine the immobilization and purification processes in one step and to save time and cost.[4]

Magnetic nanoparticles (MNPs) have also been frequently preferred as a support material for the immobilization of enzymes because of their high surface area, leading to

improved thermal stability and a higher residual activity of the immobilized enzyme under harsh solvent conditions, as compared to the free enzyme. Nevertheless, the interaction between mesoporous silica and enzyme is too weak for immobilization, so the surface functionalization must carry out with appropriate organic groups to improve stability of the immobilized enzyme.[12] In our previous works, we discovered that functionalized magnetic nanoparticles exhibited excellent results with a high immobilization yield in immobilization of enzyme.[13–16] The surface functionalization of MNPs has been carried out by binding different compounds containing functional groups such as amino (NH_2), hydroxyl (OH), carboxylic acid (COOH), or thiol (SH).[17] However, many chemical reagents used in the modification of MNPs are not only expensive but also harmful to human health and the environment.[18] Therefore, to avoid the use of these chemicals, they should be replaced with new, inexpensive and non-toxic reagents.

Tannic acid (TA) is a biocompatible water-soluble polyphenol used in applications such as different metal ions adsorption, as a polymeric coagulant and flocculants for water treatment. [19] Besides, it is used in the construction of multifunctional coatings in surface modification. Recently, TA modified carrier supports were widely used for immobilization of various enzymes such as trypsin [17,20], glucose oxidase [19], catalase [21], nitrile hydratase [22] and β-agarase.[18]

L-asparagine is a nutritional requirement for the growth of both normal and leukemia cells.[23] L-asparaginase (ASNase, EC 3.5.1.1) is important enzyme catalysis the hydrolysis of L-asparagine into aspartic acid and ammonia.[24] In presence of ASNase, the leukemia cells cannot continue to proliferate and consequently dies. The chemotherapeutic effect of the ASNase enzyme is based on this principle. However, there are two important factors limit the medical use of ASNase: First, it is a microbial product derived from *Escherichia coli* or *Erwinia chrysanthemi.*[25] Therefore, it shows a very short half-life due to rapid clearance from the body.

View Article Online
DOI: 10.1039/D0NJ00127A

Secondly, it may cause serious side effects after therapy.[26] The effective and simple method used to avoid the two disadvantages is enzyme immobilization.

Till now, many studies about the different materials as the support have been reported for ASNase immobilization. In current work, for the first time, we present in detail how the design of hybrid TA-modified magnetic particles affects the effectiveness of immobilization, activity, and performance of ASNase after immobilization. Moreover, it is also known that TA has anticancer and antioxidant properties. Therefore, the use of support containing TA for ASNase immobilization may lead to a synergistic effect. The ASNase immobilization processes on Fe_3O_4/SBA-15/TA are shown in Fig. 1. The samples were characterized by various techniques such as ATR-FTIR, XRD, VSM, SEM, EDX and zeta potential measurements. Subsequently, ASNase was successfully immobilized on Fe_3O_4/SBA-15/TA, and the biochemical properties of immobilized ASNase were investigated in detailed. As we predicted, the immobilized ASNase displayed high tolerance against extreme conditions, excellent reusability, long-term incubation stability compared to free enzyme. We hope that this detailed work will contribute to improving the immobilized ASNase in broad practical applications such as biotechnology, industrial catalysis, and biomedical engineering.

View Article Online
DOI: 10.1039/D0NJ00127A

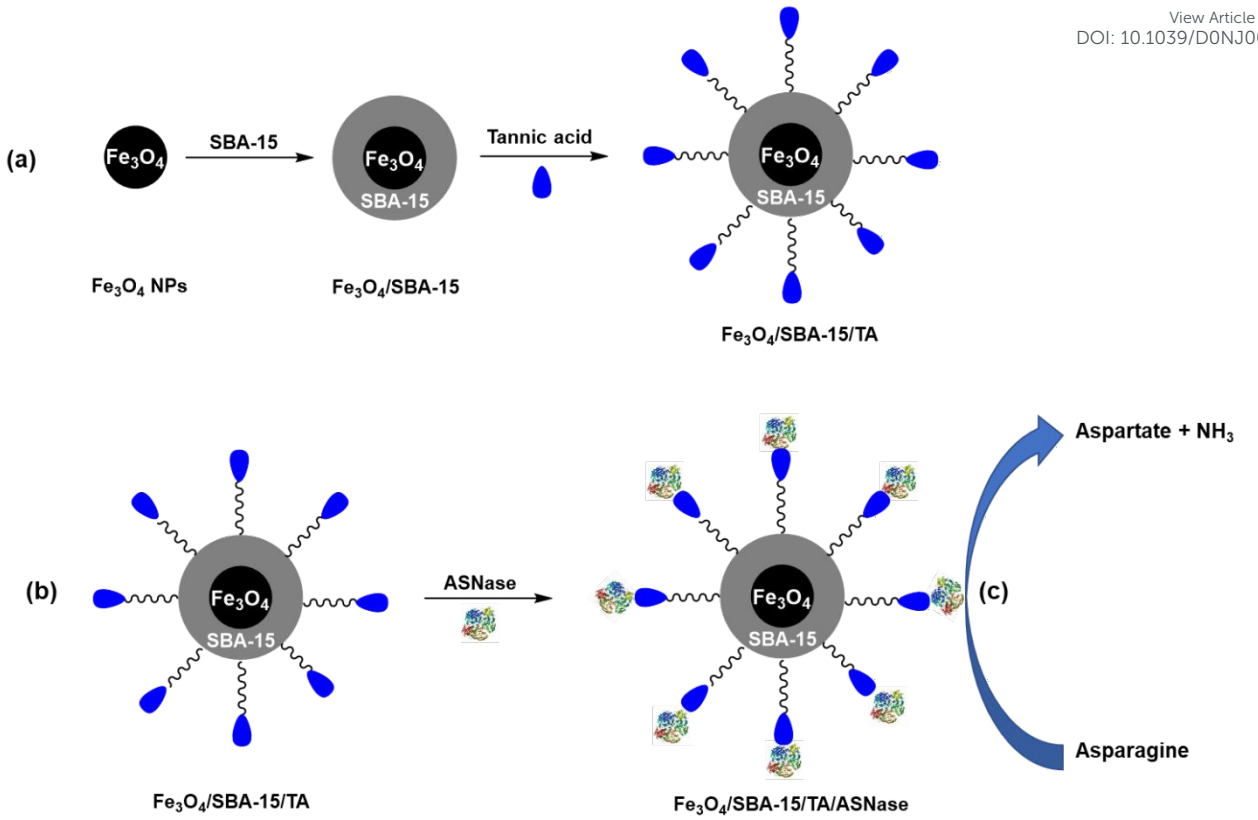

Fig. 1. The schematic diagram of the preparation of magnetic Fe_3O_4/SBA-15/TA nanoparticles (a), the immobilization of ASNase on Fe_3O_4/SBA-15/TA (b), and the catalytic activity of immobilized enzyme (c). The picture of ASNase was taken from following article.[27]

2. Materials and method

2.1. *Materials*

All the reagents were used without further purification. All enzyme and substrate solutions were freshly prepared before being used. The lyophilized ASNase powder obtained from *Escherichia coli* was purchased from ProSpec. The L-asparagine, trichloroacetic acid (TCA), tris(hydroxymethyl)aminomethane, HCl, and TA all purchased from Sigma–Aldrich. $FeCl_2 \cdot 4H_2O$, $FeCl_3 \cdot 6H_2O$, and NH_3 were obtained from Merck. The other chemicals used were of analytical purity. Ultra-pure water was used to prepare all the aqueous solutions required throughout the study.

View Article Online
DOI: 10.1039/D0NJ00127A

2.2. *Synthesis of magnetic Fe_3O_4*

Fe_3O_4 was synthesized according to method reported previously.[28] $FeCl_2 \cdot 4H_2O$ (4.23 g) and $FeCl_3 \cdot 6H_2O$ (11.48 g) were dissolved in 500 mL of distilled water, then the reaction mixture was heated to 90 °C and refluxed under Argon gas for 6 h. After that, an aqueous solution of NH_3 (25% w/v) (10 mL) was added drop by drop to the mixture over 30 min, and the reaction allowed to proceed for a further 2 h at 90 °C. The black precipitate was separated via an external magnet and washed several times with distilled water/ethanol. Fe_3O_4 particles were dried at 100 °C overnight.

2.3. *Synthesis of SBA-15*

SBA-15 mesostructured silica was prepared following the original synthesis procedure by Stucky and co-workers [29] with a modification in order to get a large-scale batch.[30,31] Pluronic P123 (PEO_{20}-PPO_{70}-PEO_{20}, M ≈5,800, Sigma-Aldrich) was used as a structure directing agent and tetraethyl orthosilicate (TEOS, 98 %, Sigma-Aldrich) as a silica source. Briefly, 1.9 M HCl was used to dissolve Pluronic P123. TEOS was added to this mixture and kept at 40 ºC for 20 h to perform a hydrolysis step. This was followed by an ageing step at 110 ºC for 24 h without stirring. The obtained SBA-15 material was filtered and calcined at 550 ºC for 5 h to remove the surfactant from the porous structure.

2.4. *Synthesis of Fe_3O_4/SBA-15 particles*

0.5 g of SBA-15 was dissolved in (25 mL) of dry toluene. A solution of Fe_3O_4 (0.25 g, 5 mL) in dry toluene was added dropwise to the dispersed SBA-15 solution under continuous stirring. The reaction mixture was kept under refluxing conditions for about 24 h under inert atmosphere by using triethylamine as initiator. Then, the product was allowed to cool at room temperature. After cooling, an external magnet was used to collect the product. After that, the product was washed several times with distilled water/ethanol and dried at 70 °C for 24 h.

View Article Online
DOI: 10.1039/D0NJ00127A

2.5. *Surface modification*

Fe_3O_4/SBA-15 (0.5 g) was dissolved in a flask containing dried acetonitrile. Afterward, TA (0.6 g) and triethylamine (0.15 ml) were added into the reaction flask. The mixture was refluxed at 80 °C for 24 h. Then, the obtained solid was separated by using an external magnet and was washed with water/ethanol for several times to remove unreacted TA. The obtained Fe_3O_4/SBA-15/TA was filtrated before drying at 60 °C overnight.[32]

2.6. *Immobilization of ASNase on Fe_3O_4/SBA-15/TA*

The obtained magnetic Fe_3O_4/SBA-15/TA particles (100 mg) were dispersed in 1 mL Tris-HCl buffer solution (50 mM, pH 8.6) by sonication. After separation, the mixture involving free enzyme (100 U) and Fe_3O_4/SBA-15/TA was directly transferred into plastic flasks. The mixed solution was incubated at 4 °C in a shaker with a continuous shaking rate (120 rpm) for 6 h until the enzyme was completely immobilized. Then, Fe_3O_4/SBA-15/TA/ASNase was separated by magnetic separation with help of an external magnet and was washed with deionized water and Tris-HCl buffer (pH 8.6) three times to remove the unbound enzymes from the supports. Finally, the Fe_3O_4/SBA-15/TA/ASNase was stored at 4 °C for activity tests.

Immobilization yield (IY) and immobilization efficiency (IE) were calculated by using Eq. (1) and Eq. (2), respectively.

$$IY\ (\%) = \frac{C^1 - C^2}{C^1} \times 100 \quad (1)$$

Where C_1 is the concentration of protein for total enzyme and C_2 is concentration of protein present in the supernatant and washing solutions after immobilization.

$$IE\ (\%) = \frac{\text{The activity of } Fe^3O^4/SBA - 15/TA/ASNase}{\text{The activity of free ASNase}} \times 100 \quad (2)$$

View Article Online
DOI: 10.1039/D0NJ00127A

2.7. *Enzymatic activity assay*

ASNase activity was measured spectrophotometrically by using L-asparagine as the substrate. Briefly, L-asparagine solution (10 mM) was prepared, first with Tris-HCl buffer (pH:8.6). A certain amount of free ASNase and Fe_3O_4/SBA-15/TA/ASNase were placed into a plastic tube, and the reaction was initiated by addition of substrate solution. The incubation time was 15 min at 37 ^oC. At the end of the time, TCA solution (1.5 M) was added to stop the reaction and 100 µl of product mixture was afterward added to 100 µl Nessler's reagent. The resulting mixture was incubated in dark for 10 min and then absorbance was measured using a microplate reader at 480 nm. One unit (U) of enzyme activity is defined as the amount of ASNase consumed to produce 1 µmol ammonia per min.

2.8. *Determination of optimal temperature and pH*

The reaction temperature and pH are important critical factors influencing the catalytic activity of enzyme. Therefore, the optimum temperature was analyzed by assaying enzyme activity after incubating the enzyme samples in the 25-70 °C range. To determine the optimum pH of free and immobilized enzyme, the activities were measured under standard assay conditions by using sodium-acetate (50 mM, pH:4.0–6.0), sodium-phosphate (50 mM, pH:7.0–8.0), and Tris-HCl (50 mM, pH:8.5-10.0) buffers.

2.9. *Thermal and storage stability*

In fact, thermal inactivation is a major challenge for industrial enzymes. Exposure to high temperatures causes changes in the 3D structure of the enzyme. Considering it's significant, the stability of free and immobilized enzyme was examined after preincubation at 50 °C for 180 min. Enzyme aliquots were removed after 30 min and the percentage of residual activities calculated.

The long-term storage stability was investigated by incubating free and immobilized enzyme under dry conditions for 28 days. The samples were withdrawn to measure the residual activity at different intervals, and the first activity was considered as 100%.

2.10. *Operational stability*

To perform the operational stability of the immobilized enzyme, a known amount of Fe_3O_4/SBA-15/TA/ASNase was transferred into a reaction tube containing substrate solution, and the reaction was performed under optimal conditions. The Fe_3O_4/SBA-15/TA/ASNase was separated from the reaction mixture via an external magnet and washed three times with Tris-HCl (pH: 8.5). After washing, the Fe_3O_4/SBA-15/TA/ASNase was subjected to repeated use by adding fresh substrate. In the first use, the relative activity was considered to be 100%.

2.11. *Determination of kinetic parameters*

Kinetic parameters (Km and Vmax) for free ASNase and Fe_3O_4/SBA-15/TA/ASNase were calculated using the Lineweaver-Burk plot at different concentrations (0.25, 0.5, 0.75, 1.0, 2.0, 4.0, 6.0, 8.0, and 10.0 mM) of L-asparagine at optimal assay conditions.

2.12. *The effects of different metal ions, inhibitors and solvents on ASNase activity*

The both free and immobilized ASNase was measured by using the assay procedure after 24 h incubation with the different metal ions (10 mM, Ag^+, Mg^{2+}, Ba^{2+}, Zn^{2+}, Hg^{2+}, Sn^{2+}, Pb^{2+}, and Al^{3+}), potential inhibitors (5%, EDTA, SDS, Tween 80 and Triton X-100) and 5% of organic solvents (acetone, acetonitrile, chloroform, tetrahydrofuran (THF), dimethylformamide (DMF) ethanol, methanol, and n-hexane).

2.13. *Instruments for characterizations*

N_2 adsorption-desorption isotherms were used to investigate the Brunauer, Emmett, and Teller (BET) surface area and Barrett-Joyner-Halenda (BJH) pore size distribution at 77 K in a

View Article Online
DOI: 10.1039/D0NJ00127A

Micromeritics Tristar 3000 apparatus for SBA-15. The surface area was obtained by using the BET equation in the P/P_0 range between 0.05 and 0.20. Pore size distribution was calculated from the adsorption branch of the isotherms through the BJH model.[33] An 8 h degasification step in nitrogen flux was performed at a temperature of 200 ºC. To detect different functional groups in samples, FTIR spectra (Perkin Elmer) were obtained in ATR mode within the wavelength range 400-4000 cm^{-1}. The XRD (Rigaku) analysis was used to analyze the structure of crystalline materials with Cu Kα radiation and the 2θ angle range of 10-80°. The saturation magnetization values of prepared particles were measured by using a VSM (PPMS) at room temperature. Knowledge about surface morphology and elemental composition of samples was taken from energy dispersive x-ray spectroscopy (EDS) in scanning electron microscopy (SEM) (LEO, 440 SEM-EDX system, Leica-Zeiss, DSM-960). The zeta potential of the samples was measured by using Zeta potential analyzer with at least 3 replicates for each sample. The enzyme activity measurements were conducted on Microplate Reader (BioTek).

2.14. *Statistical analysis*

Data were statistically analyzed using GraphPad Prism 5.0. $P<0.05$ was considered to be statistically significant.

3. Results and discussion

3.1. *Materials characterizations*

N_2 adsorption-desorption isotherm and pore size distribution of SBA-15 is shown in Fig. 2. As seen, the isotherm fits within the type IV group of isotherms corresponding to mesostructured solids, as described by the IUPAC.[33] Siliceous SBA-15 presented a wide and open porous structure. Its main textural properties are specific surface of 533 m^2/g, pore volume of 0.87 cm^3/g and a mean pore diameter of 8.5 nm. Thus, these solids present an open pore structure interesting for its further application.

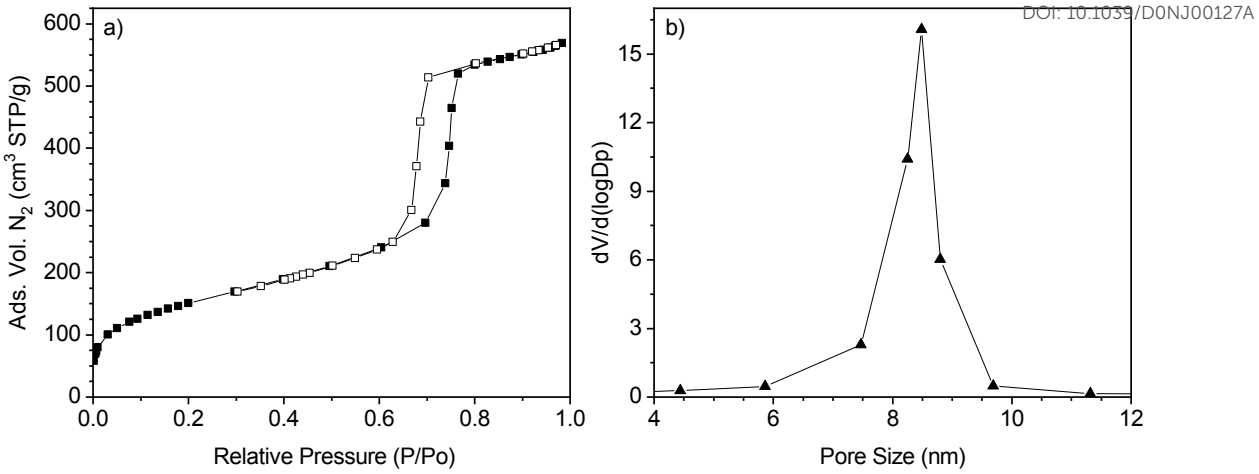

Fig. 2. a) N_2 adsorption-desorption isotherm SBA-15 silica, and b) pore size distribution of SBA-15 silica.

The FTIR spectra of Fe_3O_4, SBA-15, pure TA, and Fe_3O_4/SBA-15/TA samples are shown in Fig. 3. The band at 540 cm^{-1} are attributed to Fe–O vibration of Fe_3O_4.[34] For SBA-15, characteristic peaks strong broadband at 1000-1250 cm^{-1} and a weak band at 812 cm^{-1} are assigned to the Si-O-Si symmetric and asymmetric stretching vibration, respectively.[8] The essential characteristic bands of the pure TA compound are at 3100-3600 cm^{-1} (O-H stretching of the phenolic and methylol group of TA), 1700 cm^{-1} (C=O stretching), 1610 cm^{-1} (aromatic C=C stretching), 1191 cm^{-1} (phenolic C-O stretching), 870 cm^{-1} (the deformation out of the plane (C-H) for benzene ring band), 758 cm^{-1} (C-H vibration of benzene ring).[35] The spectrum of Fe_3O_4/SBA-15/TA contains not only the peaks of Fe_3O_4/SBA-15 but also the peaks of TA. However, the peak related to the stretching mode of the Fe-O bond shifted to shorter wavenumbers (540 and 443 cm^{-1}) after the addition of TA.[36] These results indicated that Fe_3O_4/SBA-15 was successfully coated with TA compound.

View Article Online
DOI: 10.1039/D0NJ00127A

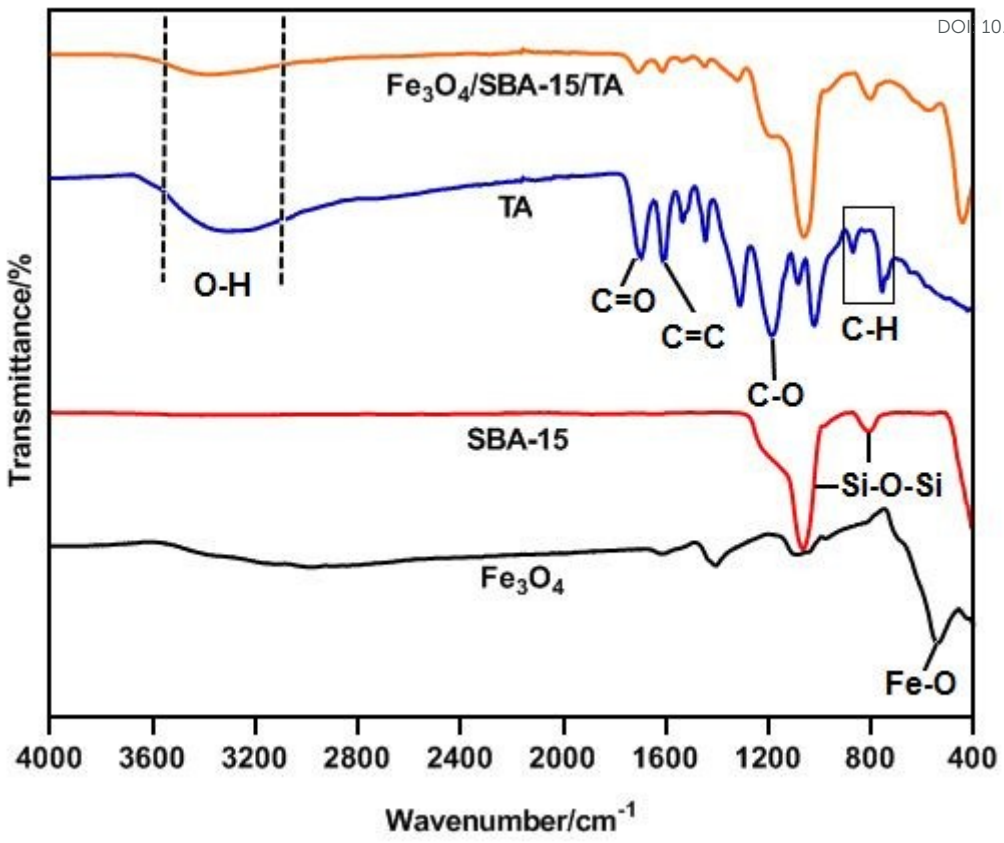

Fig. 3. FTIR spectra of Fe_3O_4 (a), SBA-15 (b), TA (c), and Fe_3O_4/SBA-15/TA (d).

The magnetic hysteresis loops for Fe_3O_4, Fe_3O_4/SBA-15, and Fe_3O_4/SBA-15/TA were shown in Fig. 4. According to the curves, the magnetization values of Fe_3O_4, Fe_3O_4/SBA-15, and Fe_3O_4/SBA-15/TA were 28.14, 8.14, and 7.94 emu g^{-1}, respectively. The saturation magnetization of the prepared Fe_3O_4 NPs was lower than the previously reported Fe_3O_4 due to size-dependent magnetization and the presence of the residues on the surface of the Fe_3O_4 NPs.[37,38] When the SBA-15 was immobilized on Fe_3O_4, the saturation magnetization was remarkably decreased. In addition, the small decrease was observed in magnetization value after covering with TA. The decreases in overall magnetization values showed that the Fe_3O_4 surface was successfully covered with nonmagnetic materials such as SBA-15 and TA.[39,40] Consequently, the Fe_3O_4/SBA-15/TA can be dispersed in aqueous solution and easily collected from aqueous solution by using an external magnet.

View Article Online
DOI: 10.1039/D0NJ00127A

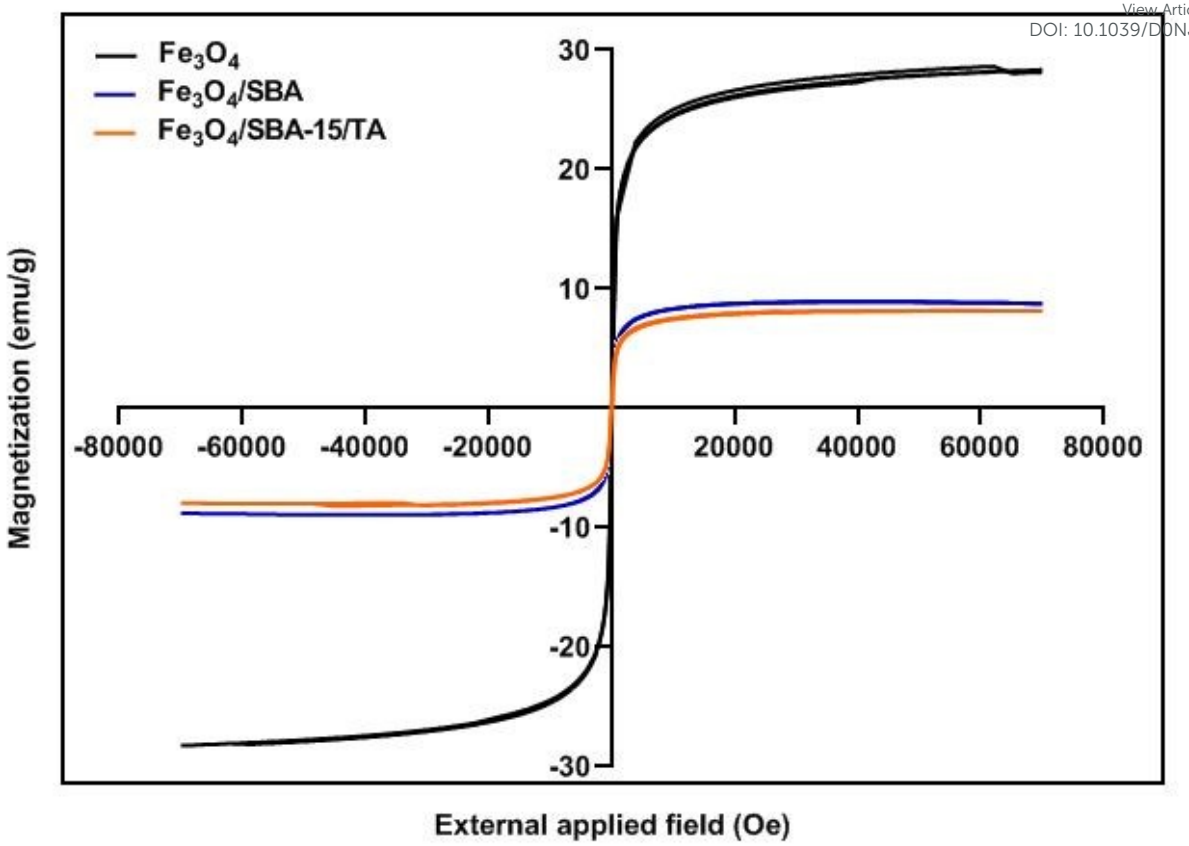

Fig. 4. Magnetic hysteresis loops of Fe_3O_4, Fe_3O_4/SBA-15, and Fe_3O_4/SBA-15/TA.

Fig. 5 showed the XRD patterns of Fe_3O_4, SBA-15, Fe_3O_4/SBA-15, and Fe_3O_4/SBA-15/TA. The six diffraction peaks observed at 30.43°, 35.56°, 43.18°, 53.35°, 57.19°, and 62.67° are well accordance with the inverse cubic spinel phase of Fe_3O_4 (Fig. 5a).[41] The strong and sharp peaks indicated well crystallization of synthesized Fe_3O_4. For SBA-15, the broad diffraction peak between 15° and 30° is ascribed to the silicon material (Fig. 5b).[40] From Fig. 5c and 5d, it can be observed that both of Fe_3O_4/SBA-15 and Fe_3O_4/SBA-15/TA showed the same pattern. However, the strong peaks for both samples compared with Fe_3O_4 were decreased due to the presence of amorphous SBA-15.[42] The XRD results verified the production of Fe_3O_4/SBA-15/TA nanocomposite.

View Article Online
DOI: 10.1039/D0NJ00127A

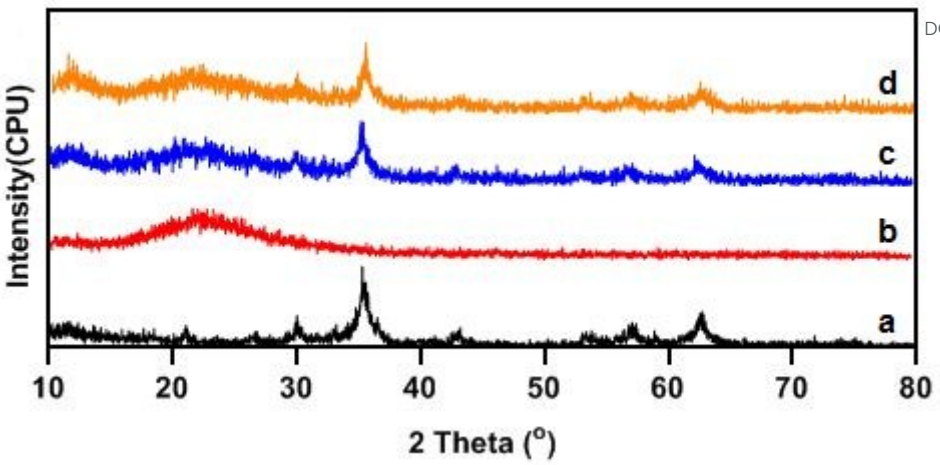

Fig. 5. XRD patterns (a) Fe_3O_4, (b) SBA-15, (c) Fe_3O_4/SBA-15 and (d) Fe_3O_4/SBA-15/TA.

3.2. *Morphological assessment*

The SEM micrographs of Fe_3O_4, SBA-15, Fe_3O_4/SBA-15, Fe_3O_4/SBA-15/TA and Fe_3O_4/SBA-15/TA/ASNase at different magnifications were shown in Fig. 6. As seen in Fig. 6a-b, the Fe_3O_4 nanoparticles displayed homogeneous size distribution and uniform morphology. However, some clusters of particles may be observed because of the magnetic interaction between the particles. Fig. 6c-d showed the typical morphology of SBA-15, and it consists of vermicular-shaped particles as described by Souza et al.[43] Although Fe_3O_4/SBA-15 particles were non-homogeneous in size, and increased surface roughness was observed due to the presence of Fe_3O_4 particles (Fig. 6e-f). As demonstrated in Fig. 6 g-h, the Fe_3O_4/SBA-15/TA displayed heterogeneous morphology, but it had still vermicular-shaped. Finally, Fig. 6i-j revealed that no significant morphological changes were observed on the surface of the material after enzyme immobilization. The obtained SEM images were similar to those previously reported in the literature.[17,44]

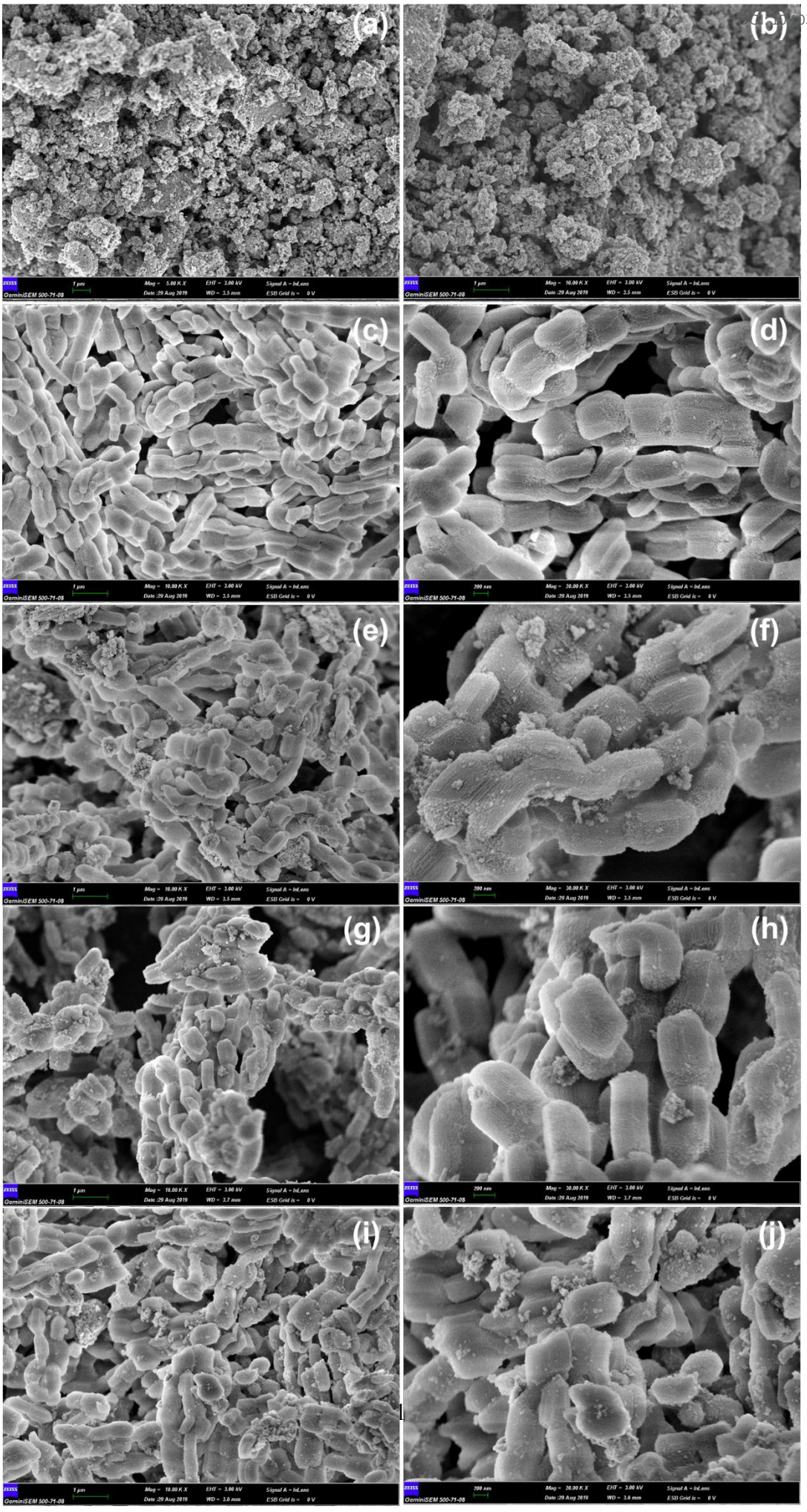

Fig. 6. SEM micrographs of (a, b) Fe_3O_4, (c, d) SBA-15, (e, f) Fe_3O_4/SBA-15, (g, h) Fe_3O_4/SBA-15/TA and (i, j) Fe_3O_4/SBA-15/TA/ASNase at different magnifications.

3.3. *EDX analysis*

The surface composition of Fe_3O_4, Fe_3O_4/SBA-15, Fe_3O_4/SBA-15/TA, and Fe_3O_4/SBA-15/TA/ASNase was determined through EDX as shown in Fig. 7. The peaks of iron (Fe) and oxygen (O) appeared in all of the samples. Fig. 7b confirmed that Fe_3O_4 was coated with SBA-15 because of in the presence of silica (Si). TA presence on the surface of Fe_3O_4/SBA-15/TA was verified by appearing of carbon (C) peak (Fig. 7c). Also, the presence of characteristic peaks of sulphur (S) and nitrogen (N) in Fig. 7d proved that ASNase was successfully immobilized onto Fe_3O_4/SBA-15/TA.

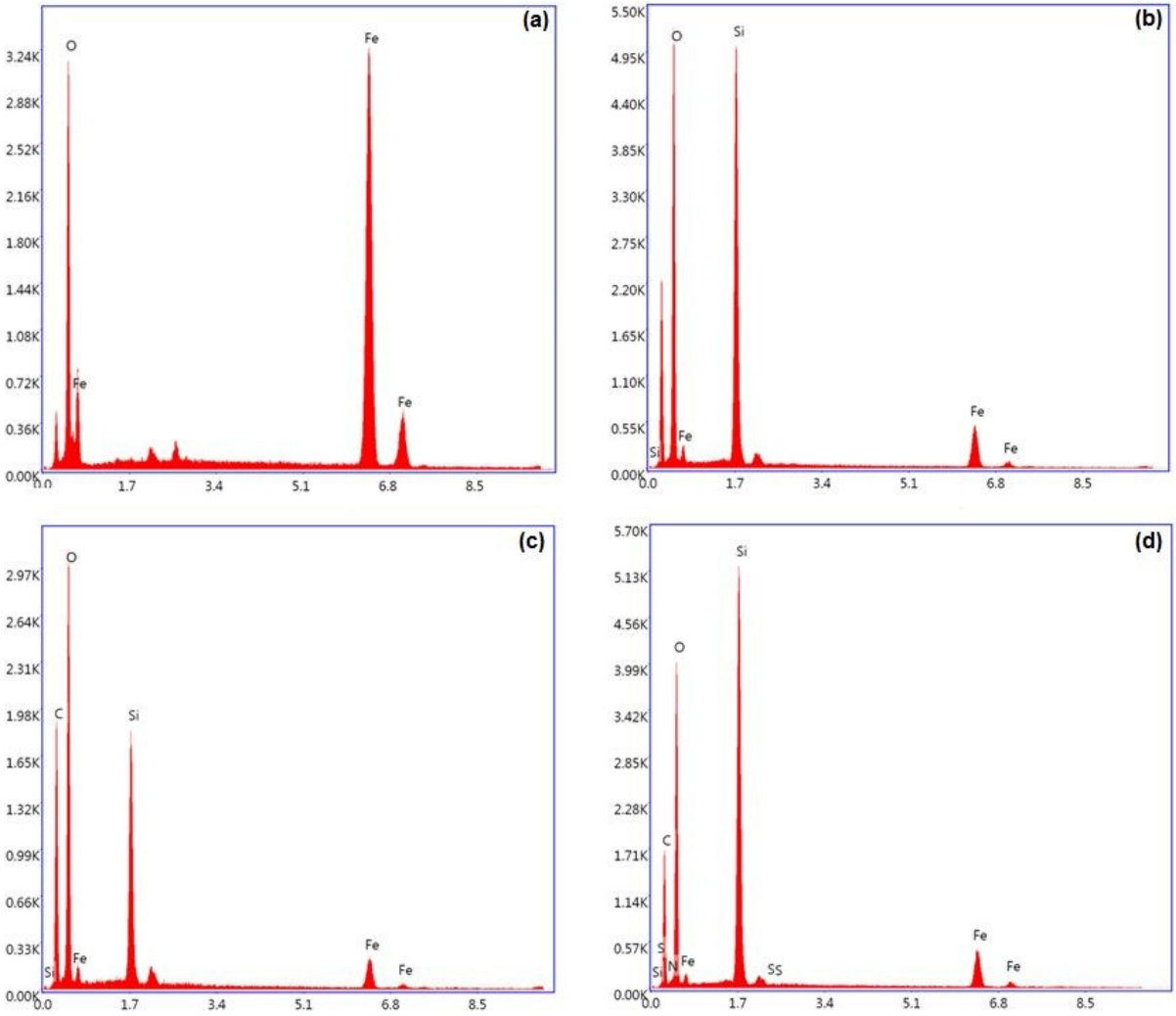

Fig. 7. EDX patterns of (a) Fe_3O_4, (b) Fe_3O_4/SBA-15, (c) Fe_3O_4/SBA-15/TA and (d) Fe_3O_4/SBA-15/TA/ASNase.

3.4. *Zeta potential*

The zeta potential values of Fe_3O_4, SBA-15, Fe_3O_4/SBA-15, and Fe_3O_4/SBA-15/TA were measured at pH:7, and each measurement was repeated three times (Fig. 8A). Fe_3O_4, SBA-15, and Fe_3O_4/SBA-15 showed a zeta potential of −32.7 mV, −30.0 mV, and -24.4, respectively. The negative charge of Fe_3O_4, SBA-15, and Fe_3O_4/SBA-15 was due to the presence of surface hydroxyl groups and silanol groups.[45,46] The zeta potential of Fe_3O_4/SBA-15/TA was -24.5 mV. The zeta potential value was not significantly changed after modification by TA at pH:7.0. In this study, Fe_3O_4/SBA-15/TA was used as support for ASNase immobilization. Therefore, we measured zeta potential values of Fe_3O_4/SBA-15/TA from pH:4.0 to 10.0 and the estimated zeta potential values were presented in Fig. 8B. As expected, the zeta potential values of Fe_3O_4/SBA-15/TA were negative in the analyzed pH range.

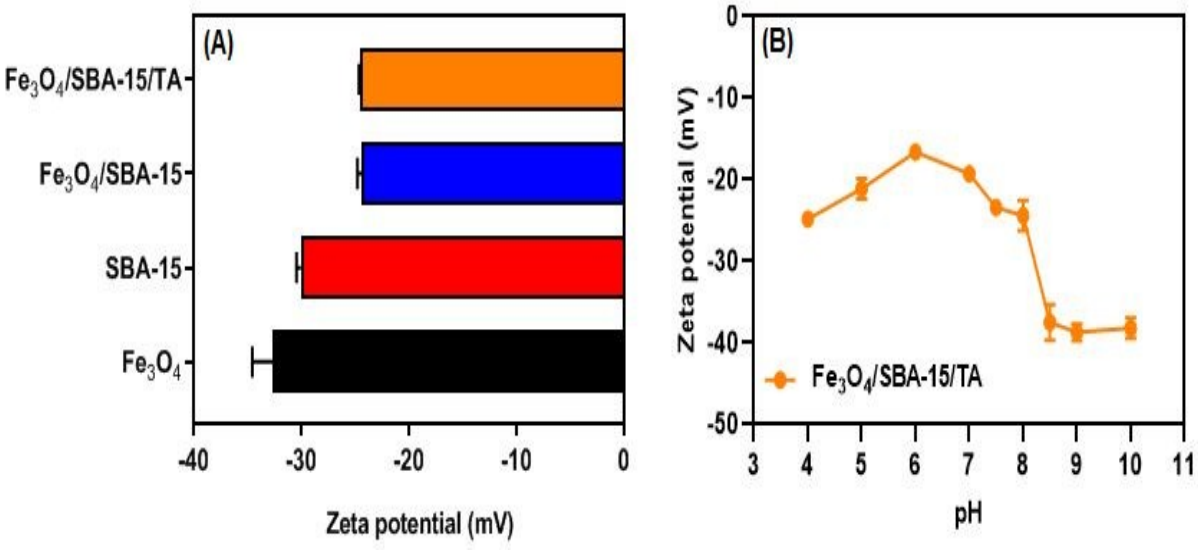

Fig. 8. Average zeta potential of Fe_3O_4, SBA-15, Fe_3O_4/SBA-15, and Fe_3O_4/SBA-15/TA at pH:7.0 and the zeta potential values of Fe_3O_4/SBA-15/TA at different pH conditions (from 4 to 10).

View Article Online
DOI: 10.1039/D0NJ00127A

3.5. *Immobilization yield and immobilization efficiency*

The Fe_3O_4/SBA-15/TA showed an immobilization yield of 92% and an immobilization efficiency of 96% for ASNase. The high immobilization efficiency and efficiency can be attributed not only to the high surface area of the nanoparticles but also to the modification of the nanoparticles with TA. Similar results were observed in studies using TA modified nanoparticles as immobilization support.[17]

3.6. *Determination of optimal pH and temperature*

The optimum temperatures of free ASNase and Fe_3O_4/SBA-15/TA/ASNase were determined, as shown in Fig. 9A. The free ASNase possessed maximum activity at 50 °C and maintained 80% of its activity at temperatures of 45 to 55 °C. At temperatures above 55 °C, the catalytic activity of free ASNase rapidly declined due to denaturation of the peptide structure and lost all activity at 65 °C. On the other hand, the activity of Fe_3O_4/SBA-15/TA/ASNase significantly improved with increasing temperature, and it exhibited its highest activity at 65 °C. In addition, the relative activity of it is more than 40% at even 70 °C. Free ASNase undergoes conformational changes with high temperature, resulting in activity decreasing at a faster rate than that of the Fe_3O_4/SBA-15/TA/ASNase.[1] In contrast, the Fe_3O_4/SBA-15/TA microenvironment protected the enzyme from denaturation under harsh conditions, and the immobilization process preserved more the enzyme stability and activity. Similar results were also obtained for the optimum pH of free ASNase and Fe_3O_4/SBA-15/TA/ASNase. As shown in Fig. 9B, free ASNase displayed maximum activity at pH 8.5, while the optimum pH of Fe_3O_4/SBA-15/TA/ASNase, as expected, shifted especially to alkaline pH range (7.5-10.0). It is well known that cationic or anionic support matrix influences the catalytic properties of enzyme after the immobilization.[47] The isoelectric point of ASNase is 8.74 and the optimum pH value is 8.50. At this pH, Fe_3O_4/SBA-15/TA possessed highly surface negative charges because of hydroxyl group on TA (zeta potential is −37.4 mV). Therefore, this shift in optimum

pH might be attributed to the microenvironment due to the weak acidity of Fe_3O_4/SBA-15/TA. The results obtained in terms of temperature and pH coincide with the data reported for both enzymes in the literature.[48,49]

3.7. *Thermal and storage stability*

To investigate thermal stability, free ASNase and its counterpart were incubated for 3 h at 50 °C (Fig. 9C). After 3 h incubation, it was observed that free ASNase lost almost half activity, while Fe_3O_4/SBA-15/TA/ASNase retained 73% of the initial activity. Thanks to Fe_3O_4/SBA-15/TA, stability and instinct structure of the enzyme were retained due to not being direct exposure to heat. It was evident from the results that hybrid composites provide a stuck protection effect and prevent denaturation under harsh conditions.[50] Similar studies reported that the thermal stability of free ASNase enhanced after immobilization. For instance, Uygun et al. reported that free ASNase maintained only 5% of its initial activity after 5 h incubation at 65 °C, whereas immobilized ASNase retained 30% of its initial activity under the same conditions.[51] In another study, trypsin was immobilized on TA modified Fe_3O_4.[17] The immobilized trypsin was found to be more thermostable than the free trypsin after 2 h incubation at 45 °C. It is indicated that the novel hybrid composite played a key role in thermal stability because of its stabilizing effect.

In terms of industrial scale, storage stability is one of the important parameters. To test the long-term storage stability of the enzymes, free and immobilized enzyme were stored at 4 °C and room temperature (nearly 25 °C). However, a slight difference between the relative activity of free ASNase and Fe_3O_4/SBA-15/TA/ASNase was observed. As shown in Fig. 9D, the Fe_3O_4/SBA-15/TA/ASNase retained about 71% of its initial activity at 4 °C and 63% at room temperature for 28 days, respectively, while free ASNase possessed 66% and 59% of the overall activity, respectively, under similar conditions. These results confirmed that the storage stability of Fe_3O_4/SBA-15/TA/ASNase improved slightly in comparison to free one after

immobilization. This might be explained by the low protective effect of the support material against denaturation and enzyme leakage.

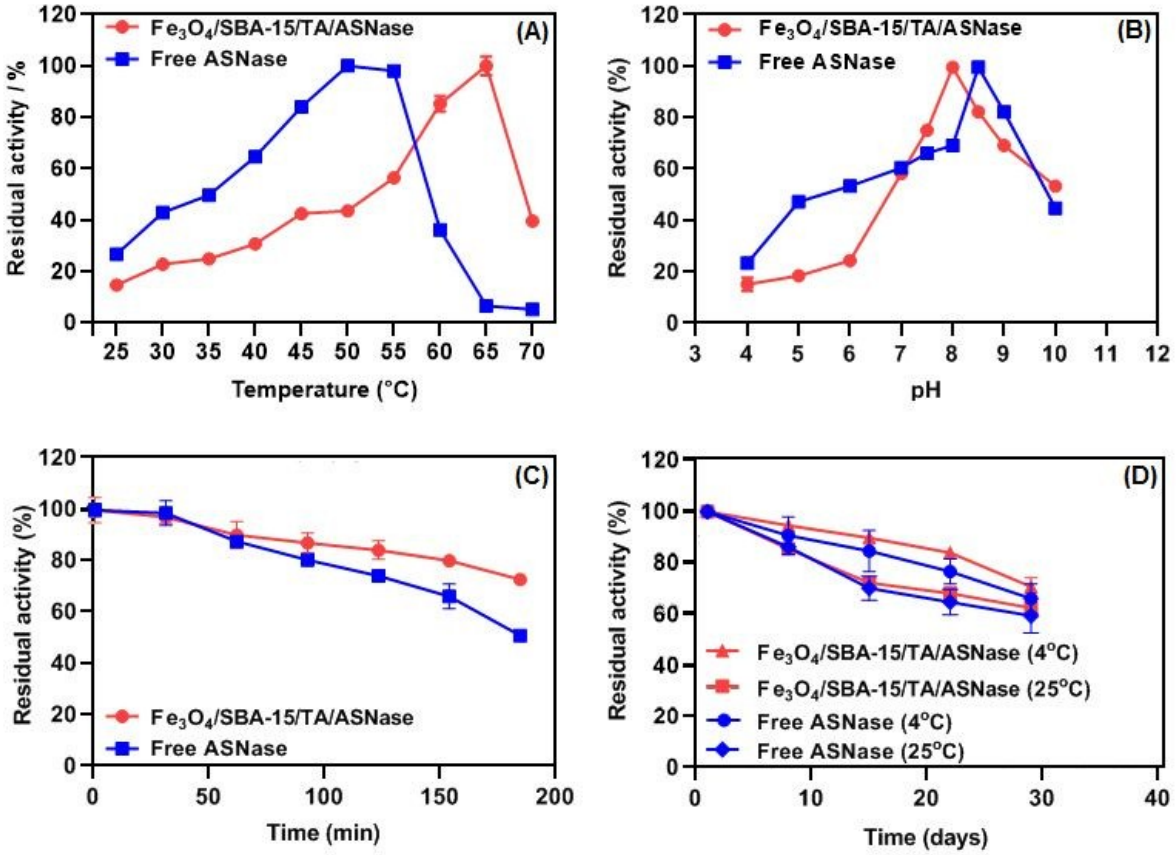

Fig. 9. (A) optimum temperature; (B) optimum pH; (C) thermal stabilities at 50 °C; (D) storage stabilities of free ASNase and Fe_3O_4/SBA-15/TA/ASNase. All measurements were run in triplicate (n=3).

3.8. *Operational stability*

Fig. 10 presents the percentages of the residual activity of the Fe_3O_4/SBA-15/TA/ASNase after multiple uses. After first 5 and 10 recycles, it maintained about 92% and 87% of its original activity, respectively. The Fe_3O_4/SBA-15/TA/ASNase exhibited better operational stability that was able to maintain 70% of the initial activity after 16 consecutive cycles. Many studies reported the reusability of immobilized ASNase on different supports. For instance, the two different immobilized ASNase maintained 42% and 29% of the initial activity after 8 cycles in

study of Monajati et al.[52] In another study, Agrawal and Kango evaluated the reusability of immobilized ASNase on the functionalized aluminum oxide nanoparticles and titanium oxide nanoparticles, and the residual activities were reported as 91.8% and 95.1%, respectively, after 9 cycles.[53] Such amazing recycling efficiency demonstrated that suggested carrier can be used in various industrial bioprocesses.

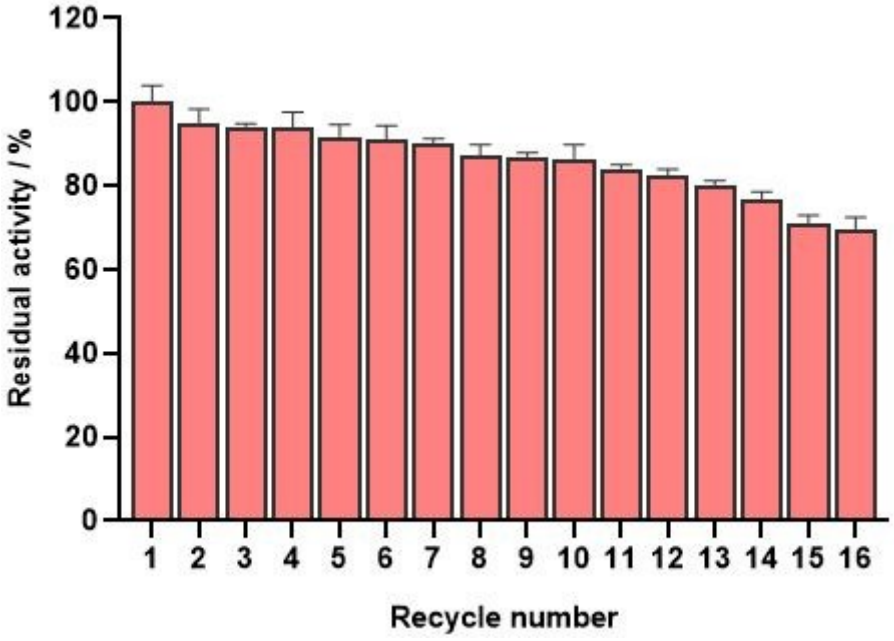

Fig. 10. The operational stability of Fe_3O_4/SBA-15/TA/ASNase. All measurements were run in triplicate (n=3).

3.9. *Determination of kinetic parameters*

The Michaelis constant (Km) and maximum reaction velocity (Vmax) was estimated by using the Lineweaver–Burk plot method at different concentrations of L-asparagine as substrate (Fig. 11). Additionally, the kinetic values were summarized in Table 1. The Km values of free ASNase and Fe_3O_4/SBA-15/TA/ASNase were calculated to be 0.34±0.03 and 0.67±0.02 mM, respectively. After ASNase immobilization, an obvious increase in Km (~1.97-fold) indicated that the Fe_3O_4/SBA-15/TA/ASNase had a significantly lower affinity for its substrate than free ASNase due to steric inhibition of the solid support. The Km was increased approximately 1.3

times for immobilized ASNase compared to free ASNase.[54] They attributed this increase to the structural changes in the enzyme or due to the lower accessibility of the substrate. On the other hand, Vmax values for free ASNase and Fe_3O_4/SBA-15/TA/ASNase were determined and this value decreased from 47.52±1.13 to 42.00±1.30 μmol min^{-1} after immobilization. The decrease in Vmax value could be due to the conformational changes in the enzyme after immobilization. Monajati prepared aspartic acid functionalized graphene oxide nanosheet for ASNase immobilization.[52] They reported that Vmax value for immobilized enzyme decreased about 1.3 times after immobilization. In another study, Uygun et al. reported a similar trend.[51] This increase in Km and decrease in Vmax are consistent with our results.

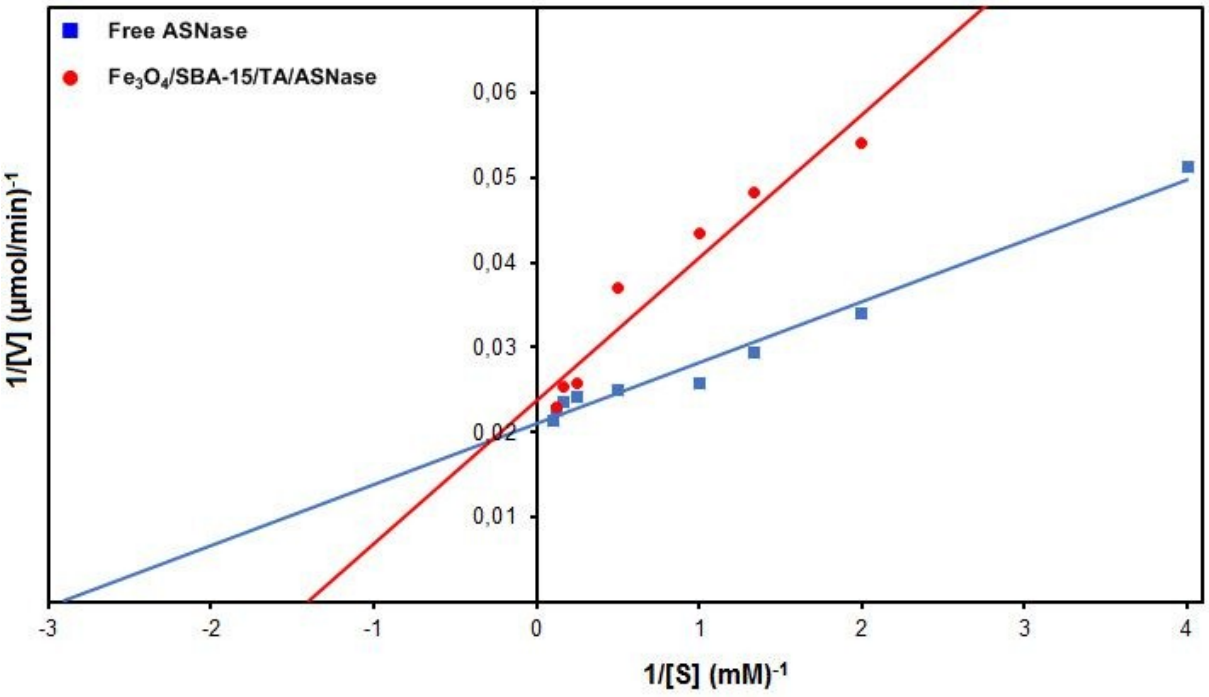

Fig. 11. The Lineweaver-Burke plots of free ASNase and Fe_3O_4/SBA-15/TA/ASNase. All measurements were run in triplicate (n=3).

Based on the Student's t-test results, Table 1 also demonstrated that the increase in Km value and the decrease in Vmax value were statistically significant at $P<0.05$.

View Article Online
DOI: 10.1039/D0NJ00127A

Table 1. Km and Vmax values of free ASNase and Fe_3O_4/SBA-15/TA/ASNase.

	Free ASNase	Fe_3O_4/SBA-15/TA/ASNase	Sig. (2-tailed)
Km (mM)	0.34±0.03	0.67±0.02	.000[a]
Vmax (μmolmin^{-1})	47.52±1.13	42.00±1.30	.000[b]

[a, b] $P<0.05$

3.10. *Effect of metal ions, inhibitors, and organic solvents*

The effects of different metal ions were studied on free ASNase and Fe_3O_4/SBA-15/TA/ASNase. The results were summarized in Table 2. The free ASNase lost 61% of its original activity in the presence of Ag^+, while silver ions showed no action on the Fe_3O_4/SBA-15/TA/ASNase (109%). On the other hand, the divalent metals tested had inhibitory effect on both free ASNase and Fe_3O_4/SBA-15/TA/ASNase except for Mg^{2+}. Zuo et al. [55] and Agrawal & Kango [53] reported that ASNase activity may be slightly stimulated in the presence of Mg^{2+}. According to our results, the relative activity of free ASNase and Fe_3O_4/SBA-15/TA/ASNase enhanced approximately 64.8% and 69.0%. Besides, this phenomenon was observed by Mahajan et al. [56] and Hassan et al. [57] Ba^{2+} (54%), Hg^{2+} (85%), Sn^{2+} (79%), Pb^{2+} (82%), Zn^{2+} (84%) and Al^{3+} (63%) showed the high inhibitory effect on free ASNase activity. Similarly, Fe_3O_4/SBA-15/TA/ASNase was also inhibited, however, it exhibited more activity in comparison to free ASNase. For instance, Fe_3O_4/SBA-15/TA/ASNase maintained high activity in presence of the strong inhibitors such as Pb^{2+} and Zn^{2+}. The highest inhibition effect was also observed with Hg^{2+} for both enzyme samples. A similar trend was reported for previous immobilized L-ASNase.[54] In another work, the ASNase was immobilized on aluminum oxide pellets. Immobilized enzyme retained 78% of its initial activity in presence 5 mM Hg^{2+}, whereas the free ASNase maintained 41% of its initial activity [58]. These inhibitions may be due to

charged ions interact with the side chain groups of amino acids in the enzyme which affects the conformation and stability of the enzyme.[59]

Table 2. The effects of different metal ions on free ASNase and Fe_3O_4/SBA-15/TA/ASNase activity. All measurements were run in triplicate (n=3).

Metal ions	**Concentration**	**Relative activity (%)**	
		Free ASNase	**Fe_3O_4/SBA-15/TA/ASNase**
Control	-	100±4.1	100±12.1
Ag^{+}	10 mM	39.2±6.6	109.9±5.9
Mg^{2+}	10 mM	164.8±8.9	169±16.5
Ba^{2+}	10 mM	46.0±0.7	76.2±8.0
Hg^{2+}	10 mM	15.4±2.4	54.7±2.8
Sn^{2+}	10 mM	21.3±0.3	79.0±3.9
Pb^{2+}	10 mM	18.4±1.5	59.6±2.7
Zn^{2+}	10 mM	16.0±1.1	61.6±5.1
Al^{3+}	10 mM	37.2±2.4	68.5±1.1

As shown in Fig. 12A, the stability of free ASNase and Fe_3O_4/SBA-15/TA/ASNase were investigated in the presence of various inhibitors. The results revealed that the relative activity of free ASNase significantly decreased in EDTA, SDS, Tween 80 and Triton X-100 by about 83%, 63%, 71% and 66%, respectively. Although the relative activity of the Fe_3O_4/SBA-15/TA/ASNase decreased by about 31% in Triton X-100, its relative activity almost stable in the presence of SDS and Tween 80. El-Naggar et al. investigated the effect of several inhibitors on the purified L-asparaginase from *Streptomyces brollosae* NEAE-115 [60]. They reported that Tween 80 acted as activators for ASNase activity. This increase was also in agreement with our

result. Surprisingly, its relative activity significantly increased by about 1.5-fold after EDTA incubation. A similar enhancement was reported for ASNase immobilization on titanium oxide nanoparticles. The relative activity was increased approximately 40% compared to control (100%), which is similar with our results.[53]

The effects of different organic solvents on the activity of free ASNase and Fe_3O_4/SBA-15/TA/ASNase were also investigated, and the results are shown in Fig. 12B. After 24 h of incubation, the residual activity of free ASNase was 80.8, 87.3, 53.0, 71.7 and 93.6%, whereas Fe_3O_4/SBA-15/TA/ASNase maintained 95.5, 111.5, 113.1, 104.4, 107.8% of its initial activity in chloroform, DMF, THF, ethanol and n-hexane, respectively. However, interestingly, a noticeable increase in Fe_3O_4/SBA-15/TA/ASNase activity was observed approximately 23.8, 28.1, and 57.6% in the presence of methanol, acetone, and acetonitrile, respectively. Similar findings related to organic solvents stability for immobilized enzyme was also reported by Agrawal and Kango [53] and Agrawal et al. [58]. The modified ASNase showed relative activity 168, 138, 114, 112 and 107% in presence of ethyl acetate, acetone, acetonitrile, ethanol and methanol by respectively. These results are in good agreement with our outcome in terms of organic solvents stability tests.

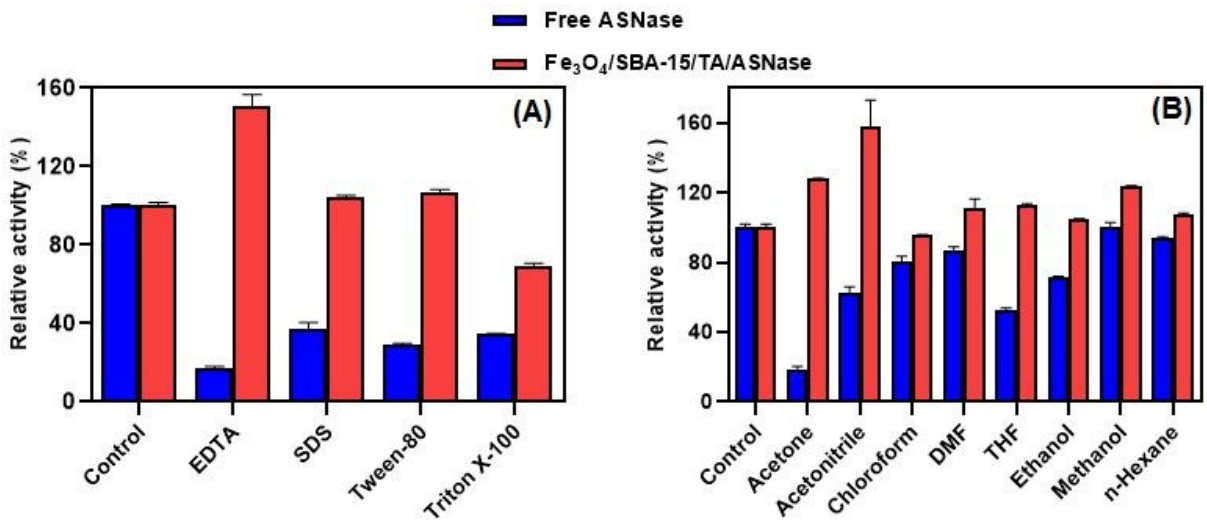

Fig. 12. The effects of different inhibitors (A) and organic solvents (B) on the activity of free ASNase and Fe_3O_4/SBA-15/TA/ASNase. All measurements were run in triplicate (n=3).

4. Conclusions

In summary, the present work demonstrated the successful immobilization of ASNase on the Fe_3O_4/SBA-15 support functionalized with TA to improve stability and biochemical properties of ASNase. The use of the Fe_3O_4/SBA-15/TA for ASNase immobilization is important in two aspects. On the one hand, thanks to the functional groups on surface, ASNase was immobilized quickly and easily on these surfaces as a result of interactions. On the other hand, Fe_3O_4/SBA-15/TA can be rapidly separated and propelled from the reaction system to provide practical and low-cost applications. In this respect, the carrier matrix was verified via ATR-FTIR, SEM, EDX, VSM, and XRD analysis. A significant improvement in pH and thermal stability of Fe_3O_4/SBA-15/TA/ASNase was observed when compared to its free counterpart. Additionally, the Fe_3O_4/SBA-15/TA/ASNase exhibited high thermal stability, repeated usage as well as extended storage. However, the drawbacks of this support can be summarized as follows: (1) As expected, slight loss of activity was observed due to mass transfer limitations after immobilization. (2) It is very well known that adsorption has disadvantages such as enzyme leakage from the support material, activity loss and contamination of the product. Despite these disadvantages, the results show that the Fe_3O_4/SBA-15/TA material can be satisfactorily applied to biomedical, drug delivery systems, cell/enzyme immobilization, and many other related areas. Also, further studies on the immobilization of different biocatalysts are under way.

Disclosure statement

No potential conflict of interest was reported by the authors.

References

1 A. Samui and S. K. Sahu, *New J. Chem*., 2018, 42, 4192-4200.

2 J. Song, H. Shen, Y. Yang, Z. Zhou, P. Su and Y. Yang, *J. Mater. Chem. B*, 2018, **6**, 5718-5728.

3 S. Kumar-Krishnan, A. Hernandez-Rangel, U. Pal, O. Ceballos-Sanchez, F. J. Flores-Ruiz, E. Prokhorov, O. Arias De Fuentes, R. Esparza and M. Meyyappan, *J. Mater. Chem. B*, 2016, **4**, 2553-2560.

4 Ö. Acet, N. H. Aksoy, D. Erdönmez and M. Odabaşı, *Artif. Cells, Nanomedicine Biotechnol*., 2018, **46**, 538-545.

5 D. Zhao, Q. Huo, J. Feng, B. F. Chmelka and G. D. Stucky, *J. Am. Chem. Soc.*, 1998, **120**, 6024-6036.

6 N. S. Rios, M. P. Pinheiro, M. L. B. Lima, D. M. G. Freire, I. J. da Silva, E. Rodríguez-Castellón, H. B. de Sant'Ana, A. C. Macedo and L. R. B. Gonçalves, *Chem. Eng. Res. Des*., 2018, **129**, 12-24.

7 P. Van Der Voort, P. I. Ravikovitch, K. P. De Jong, M. Benjelloun, E. Van Bavel, A. H. Janssen, A. V. Neimark, B. M. Weckhuysen and E. F. Vansant, *J. Phys. Chem. B*, 2002, **106**, 5873-5877.

8 Ö. Acet, B. Önal, R. Sanz, E. S. Sanz-Pérez, D. Erdönmez and M. Odabaşi, *J. Mol. Liq*., 2019, **276**, 480-487.

9 Z. Wu and D. Zhao, *Chem. Commun*., 2011, **47**, 3332–3338.

10 S. H. Joo, J. Y. Park, C. K. Tsung, Y. Yamada, P. Yang and G. A. Somorjai, *Nat. Mater*., 2009, **8**, 126-131.

11 B. Önal, Ö. Acet, R. Sanz, E. S. Sanz-Pérez, D. Erdönmez and M. Odabaşi, *Int. J. Biol. Macromol.*, 2019, **141**, 1183-1190.

12 N. Lin, L. Gao, Z. Chen and J. H. Zhu, *New J. Chem.*, 2011, **35**, 1867-1875.

13 A. Ulu, S. A. A. Noma, S. Koytepe and B. Ates, *Artif. Cells, Nanomedicine Biotechnol.*, 2018, **46**, 1035-1045.

14 A. Ulu, I. Ozcan, S. Koytepe and B. Ates, *Int. J. Biol. Macromol.*, 2018, **115**, 1122-1130.

15 B. Ates, A. Ulu, S. Köytepe, S. A. Ali Noma, V. S. Kolat and T. Izgi, *RSC Adv.*, 2018, **8**, 36063-36075.

16 A. Ulu, S. A. A. Noma, S. Koytepe and B. Ates, *Appl. Biochem. Biotechnol.*, 2018, **187**, 938-956.

17 K. Atacan and M. Özacar, *Colloids Surfaces B Biointerfaces*, 2015, **128**, 227–236.

18 Q. Xiao, C. Liu, H. Ni, Y. Zhu, Z. Jiang and A. Xiao, *Food Chem.*, 2019, **272**, 586-595.

19 S. Altun, B. Çakiroğlu, M. Özacar and M. Özacar, *Colloids Surfaces B Biointerfaces*, 2015, **136**, 963-970.

20 K. Atacan, B. Çakiroğlu and M. Özacar, *Food Chem.*, 2016, **212**, 460-468.

21 J. Cui, S. Ren, T. Lin, Y. Feng and S. Jia, *Chem. Eng. J.*, 2018, **343**, 629-637.

22 J. kai Gao, Z. jun Zhang, Y. jun Jiang, Y. Chen and S. feng Gao, *Molecules*, 2017, **22**, 1597.

23 K. Kumar, J. Kaur, S. Walia, T. Pathak and D. Aggarwal, *Leuk. Lymphoma*, 2014, **55**, 256–62.

24 L. P. Brumano, F. V. S. da Silva, T. A. Costa-Silva, A. C. Apolinário, J. H. P. M. Santos, E. K. Kleingesinds, G. Monteiro, C. de O. Rangel-Yagui, B. Benyahia and A. P. Junior, *Front. Bioeng. Biotechnol.*, 201, **6**, 212.

25 N. E. A. El-Naggar, S. M. El-Ewasy and N. M. El-Shweihy, *Int. J. Pharmacol*., 2014, **10**, 182-199.

26 X. Thomas and C. Le Jeune, *Int. J. Hematol. Oncol*., 2016, **5**, 11.

27 D. S. Wishart, Y. D. Feunang, A. C. Guo, E. J. Lo, A. Marcu, J. R. Grant, T. Sajed, D. Johnson, C. Li, Z. Sayeeda, N. Assempour, I. Iynkkaran, Y. Liu, A. MacIejewski, N. Gale, A. Wilson, L. Chin, R. Cummings, Di. Le, A. Pon, C. Knox and M. Wilson, *Nucleic Acids Res*., 2018, **46**, D1074-D1082.

28 J. Mondal, T. Sen and A. Bhaumik, *Dalt. Trans*., 2012, **41**, 6173.

29 D. Zhao, J. Feng, Q. Huo, N. Melosh, G. Fredrickson, B. Chmelka and G. Stucky, *Science*, 1998, **279**, 548–552.

30 E. S. Sanz-Pérez, A. Fernández, A. Arencibia, G. Calleja and R. Sanz, *Chem. Eng. J.,* 2019, **373**, 1286–1294.

31 E. S. Sanz-Pérez, A. Arencibia, R. Sanz and G. Calleja, *RSC Adv*., 2015, **5**, 103147-103154.

32 A. Feiz, M. M. Amini and A. Bazgir, *Mol. Catal*., 2017, **438**, 159–166.

33 M. Thommes, K. Kaneko, A. V. Neimark, J. P. Olivier, F. Rodriguez-Reinoso, J. Rouquerol and K. S. W. Sing, *Pure Appl. Chem*., 2015, **87**, 1051–1069.

34 M. Kumari, Y. Jain, P. Yadav, H. Laddha and R. Gupta, *Catal. Letters*, 2019, **149**, 2180-2194.

35 S. Çakar and M. Özacar, *Spectrochim. Acta - Part A Mol. Biomol. Spectrosc.*, 2016, **163**, 79-88.

36 A. F. M. Santos, L. J. A. Macedo, M. H. Chaves, M. Espinoza-Castañeda, A. Merkoçi, F. D. C. A. Limac and W. Cantanhêde, *J. Braz. Chem. Soc*., 2016, **163**, 79-88.

37 W. Chen, P. Yi, Y. Zhang, L. Zhang, Z. Deng and Z. Zhang, *ACS Appl. Mater. Interfaces*, 2011, **3**, 4085–4091.

38 G. Kandasamy and D. Maity, *Int. J. Pharm*., 2015, **496**, 191-218.

39 S. Yang, T. Zeng, Y. Li, J. Liu, Q. Chen, J. Zhou, Y. Ye and B. Tang, *J. Nanomater*., 2015, 817924.

40 A. Maleki, M. Rabbani and S. Shahrokh, *Appl. Organomet. Chem*., 2015, **29**, 809-814.

41 V. A. J. Silva, P. L. Andrade, M. P. C. Silva, A. D. Bustamante, L. De Los Santos Valladares and J. Albino Aguiar, *J. Magn. Magn. Mater*., 2013, **343**, 138-143.

42 N. N. Song, H. T. Yang, H. L. Liu, X. Ren, H. F. Ding, X. Q. Zhang and Z. H. Cheng, *Sci. Rep*., 2013, **3**, 3161.

43 K. C. Souza, J. D. Ardisson and E. M. B. Sousa, *J. Mater. Sci. Mater. Med*., 2019, **20**, 512.

44 H. Aliyan, R. Fazaeli and R. Jalilian, *Appl. Surf. Sci*., 2013, **276**, 147-153.

45 H. Li, M. Zhai, H. Chen, C. Tan, X. Zhang and Z. Zhang, *Materials (Basel)*. 2019, **12**, 546.

46 J. Zou, Y. G. Peng and Y. Y. Tang, *RSC Adv.*, 2014, **4**, 9693–9700

47 M. A. Nawaz, A. Karim, Z. Bibi, H. U. Rehman, A. Aman, D. Hussain, M. Ullah and S. A. U. Qader, *J. Taiwan Inst. Chem. Eng*., 2016, **64**, 31-38.

48 A. Ulu, S. Koytepe and B. Ates, *Carbohydr. Polym*., 2016, **153**, 559–572.

49 A. Ulu, S. Koytepe and B. Ates, *J. Appl. Polym. Sci*., 2016, **133**.

50 Y. Li, T. Jing, G. Xu, J. Tian, M. Dong, Q. Shao, B. Wang, Z. Wang, Y. Zheng, C. Yang and Z. Guo, *Polymer*, 2018, **149**, 13-22.

51 M. Uygun, B. Jurado-Sánchez, D. A. Uygun, V. V. Singh, L. Zhang and J. Wang, *Nanoscale*, 2017,**9**, 18423-18429.

52 M. Monajati, S. Borandeh, A. Hesami, D. Mansouri and A. M. Tamaddon, *Chem. Eng. J.*, 2018, 354, 1153-1163.

53 S. Agrawal and N. Kango, *Int. J. Biol. Macromol*., 2019, **135**, 1142–1150.

54 H. A. El-Refai, M. S. Shafei, H. Mostafa, A. M. H. El-Refai, E. M. Araby, F. M. El-Beih, S. M. Easa and S. K. Gomaa, *Polish J. Microbiol*., 2016, **65**, 43–50.

55 S. Zuo, T. Zhang, B. Jiang and W. Mu, *Extremophiles*, 2015, **19**, 841-851.

56 R. V. Mahajan, V. Kumar, V. Rajendran, S. Saran, P. C. Ghosh and R. K. Saxena, *PLoS One*, 2014, **9**, e99037.

57 S. W. M. Hassan, A. M. Farag and E. A. Beltagy, *J. Pure Appl. Microbiol*., 2018, 5284.

58 S. Agrawal, I. Sharma, B. P. Prajapati, R. K. Suryawanshi and N. Kango, *Int. J. Biol. Macromol*., 2018, **114**, 504–511.

59 A. Ugur, N. Sarac, R. Boran, B. Ayaz, O. Ceylan and G. Okmen, *ISRN Biochem*., 2014, **2014**, 289749.

60 N. E. A. El-Naggar, S. F. Deraz, S. M. El-Ewasy and G. M. Suddek, *BMC Pharmacol. Toxicol.*, 2018, **19**, 51.

View Article Online
DOI: 10.1039/D0NJ00127A

A Table of Contents Entry

Herein, we report the preparation of tannic acid modified magnetic Fe_3O_4/SBA-15 nanoparticles and its application as a carrier matrix for immobilization of ASNase anticancer enzyme-drug.